Revista Mexicana de Astronomía y Astrofísica, **48**, 209–222 (2012)

NEW ANALYTIC RESULTS FOR POISSONIAN AND NON-POISSONIAN STATISTICS OF COSMIC VOIDS

L. Zaninetti

Dipartimento di Fisica, Universitá degli Studi di Torino, Italy

Received 2012 January 10; accepted 2012 April 10

RESUMEN

La estereología permite pasar de las distribuciones en 3D de los volúmenes en los diagramas de Voronoi a sus secciones transversales en 2D. La suposición básica es que la estadística en 3D de los volúmenes de los vacíos en el Universo local obedece a una función de distribución de tipo gama. La regla estándar para pasar de volúmenes en 3D a círculos en 2D mediante la estereología común produce una nueva función de densidad de probabilidad para los radios, la cual contiene la función G de Meijer. También se considera una distribución no Poissoniana para los volúmenes. El mejor ajuste para la distribución de los radios en 3D del Sloan Digital Sky Survey Data Release 7 es una distribución no Poissoniana de los volúmenes, dada por la función de Kiang con argumento cercano a dos.

ABSTRACT

Stereology allows shifting from the 3D distribution of the volumes of Poissonian Voronoi Diagrams to their 2D cross-sections. The basic assumption is that the 3D statistics of the volumes of the voids in the local Universe has a distribution function of the gamma-type. The standard rule of conversion from 3D volumes to 2D circles, adopting the standard rules of stereology, produces a new probability density function of the radii which contains the Meijer G-function. A non-Poissonian distribution of volumes is also considered. The distribution of the 3D radii of the Sloan Digital Sky Survey Data Release 7 is best fitted by a non-Poissonian distribution in volumes as given by the Kiang function with argument of about two.

Key Words: galaxies: clusters: general — galaxies: statistics — large-scale structure of universe — methods: statistical

1. INTRODUCTION

The astronomical analysis of the cellular nature of the large scale structure of our universe started with the second CFA2 redshift Survey which produced slices showing that the spatial distribution of galaxies is not random but is organized in filaments which represent the 2D projection of 3D bubbles, see Geller & Huchra (1989). The organization of astronomical observations continued with the 2dF Galaxy Redshift Survey (2dFGRS), see Colless et al. (2001), and with the Sloan Digital Sky Survey (SDSS), see York et al. (2000); Abazajian et al. (2009). These catalogs of slices allow the determination of the size of the voids as approximated by circles of a given radius. A visual inspection of these slices allows a rough evaluation of the largest void, which turns to be ≈34/h Mpc. A refined statistics requires a digital version of the radii as given by the catalog of cosmic voids of SDSS R7 (Pan et al. 2011).

A possible approach to the statistics of these voids is given by the Voronoi tessellation, after the two historical papers by Voronoi (1907, 1908).

Following the nomenclature introduced by Okabe, Boots, & Sugihara (1992), we call the intersection between a plane and the Poissonian Voronoi tessellation (PVT) $V_p(2,3)$. We briefly recall that the first application of the PVT to astrophysics is due to Kiang (1966). The applications of Voronoi Diagrams to galaxies started with

Icke & van de Weygaert (1987), where a sequential clustering process was adopted in order to insert the initial seeds, and continued with van de Weygaert & Icke (1989), Pierre (1990), Barrow & Coles (1990), Coles (1991), van de Weygaert (1991a,b), Zaninetti (1991), Ikeuchi & Turner (1991), Subba Rao & Szalay (1992), van de Weygaert (1994), Goldwirth, da Costa, & van de Weygaert (1995), van de Weygaert (2002, 2003), Zaninetti (2006). An updated review of 3D Voronoi Diagrams applied to cosmology can be found in van de Weygaert (2002, 2003). The 3D PVT can also be applied to identify groups of galaxies in the structure of a super-cluster, see Ebeling & Wiedenmann (1993), Bernardeau & van de Weygaert (1996), Schaap & van de Weygaert (2000), Marinoni et al. (2002), Melnyk, Elyiv, & Vavilova (2006), van de Weygaert & Schaap (2009), Elyiv, Melnyk, & Vavilova (2009).

A different approach to the intersections between bubbles and a plane is given by stereology, which is the science of the geometrical relationships between structures that exists in three dimensions (3D) and their images, which are fundamentally two-dimensional (2D). The absence of a probability density function (PDF) for the main parameters of the PVT area in 2D and the volume in 3D has hindered the development of a PDF in radii of the $V_p(2,3)$ problem. The publication with a relative test of a new PDF for the cell of PVT as given by Ferenc & Néda (2007), allows a simple parametrization of the cell. The integral connected with the $V_p(2,3)$ problem can now be expressed in analytical terms rather than numerical. The previous comments can also be rewritten in the form of some key questions.

- Is it possible to derive the probability density function for the radii of 2D sections in the Poissonian case?
- Is it possible to obtain an analytic expression for the survival function, see equation (29), of the radii of 2D sections in the Poissonian case?
- Is it possible to derive analytic results for the radii of 2D sections in the case of non-Poissonian seeds or volumes?
- Can we apply the obtained analytic results to the catalog of cosmic voids as given, for example, by the SDSS R7?

In this paper we analyze in § 2 the two main PDFs adopted in order to model the cells of PVT which are the old but still widely used Kiang function (Kiang 1966) and the recent Ferenc-Néda function (Ferenc & Néda 2007). § 3 reviews the probability of a plane intersecting a given sphere, the stereological approach, and then inserts in the fundamental integral of the stereology the cell's radius of the new PDF. § 4 contains the observed statistics of 1054 cosmic voids, a theoretical comparison with the radii of PVT and a comparison of the observed survival function of 2dFGRS with our survival function as given by the stereology. An example of non-Poissonian Voronoi Tessellation (NPVT) statistics in the light of the Kiang function is given in § 5.

2. THE DISTRIBUTIONS ADOPTED FOR PVT

We briefly review the PDFs which regulate the main parameters of PVTs: area in 2D, and volume in 3D.

2.1. *The Kiang function*

The gamma variate $H(x;c)$ (Kiang 1966) is

$$H(x;c) = \frac{c}{\Gamma(c)}(cx)^{c-1}\exp(-cx)\,, \tag{1}$$

where $0 \leq x < \infty$, $c > 0$, and Γ is the gamma function. The Kiang PDF has a mean of

$$\mu = 1\,, \tag{2}$$

and a variance

$$\sigma^2 = \frac{1}{c}\,. \tag{3}$$

In the case of a 1D PVT, $c = 2$ is an exact analytic result and conversely c is supposed to be 4 or 6 for 2D or 3D PVTs, respectively, the so called Kiang conjecture (Kiang 1966).

TABLE 1

VALUES OF χ^2 FOR THE CELL NORMALIZED AREA-DISTRIBUTION FUNCTION IN 2D AND THE CELL NORMALIZED VOLUME-DISTRIBUTION FUNCTION IN 3D[a]

Dimension	PDF	Parameters	χ^2
2D	$H(x;c)$ (equation 1)	$c = 3.55$	83.48
2D	$f(x;d)$ (equation 4)	$d = 2$	71.83
3D	$H(x;c)$ (equation 1)	$c = 5.53$	93.86
3D	$f(x;d)$ (equation 4)	$d = 3$	134.15

[a]Here T_i are the theoretical frequencies and O_i are the sample frequencies. We have 25 087 Poissonian seeds in 2D, 21 378 Poissonian seeds in 3D, and 40 intervals in the histogram.

2.2. *Ferenc-Néda function*

A new PDF has been recently introduced (Ferenc & Néda 2007), in order to model the normalized area/volume in 2D/3D PVT

$$FN(x;d) = C \times x^{3d-1/2} \exp\left(-(3d+1)x/2\right), \tag{4}$$

where C is a constant,

$$C = \frac{\sqrt{2}\sqrt{3\,d+1}}{2\,2^{3/2\,d}\,(3\,d+1)^{-3/2\,d}\,\Gamma\left(3/2\,d+1/2\right)}, \tag{5}$$

and d ($d = 1, 2, 3$) is the dimension of the space under consideration. We will call this function the Ferenc-Néda PDF; it has a mean of

$$\mu = 1, \tag{6}$$

and a variance

$$\sigma^2 = \frac{2}{3d+1}. \tag{7}$$

The Ferenc-Néda PDF can be obtained from the Kiang function (Kiang 1966) by the transformation

$$c = \frac{3d+1}{2}. \tag{8}$$

2.3. *Numerical results*

In the following, we will model the PVT in which the seeds are computed through a random process. The χ^2 is computed according to the formula

$$\chi^2 = \sum_{i=1}^{N} \frac{(T_i - O_i)^2}{T_i}, \tag{9}$$

where N is the number of bins, T_i is the theoretical value, and O_i is the experimental value. A first test of the PDFs presented in the previous section can be made by analyzing the Voronoi cell normalized area-distribution in 2D and normalized volume-distribution in 3D, see Table 1.

In this comparison $f(x;d)$ by Ferenc & Néda (2007), the number of free parameters is zero because $d = 2$ or $d = 3$ fixes the distribution. In the case of $H(x;c)$ by Kiang (1966), we have one free parameter which is fixed by the sample.

3. STEREOLOGY

We first briefly review how a PDF $f(x)$ changes to $g(y)$ when a new variable $y(x)$ is introduced. We limit ourselves to the case in which $y(x)$ is a one-to-one transformation. The rule for transforming a PDF is

$$g(y) = \frac{f(x)}{|\frac{dy}{dx}|}\,. \tag{10}$$

Analytic results have shown that sections through D-dimensional Voronoi tessellations are not themselves D-1 Voronoi tessellations (Møller 1989, 1994; Chiu, Weygaert, & Stoyan 1996). According to Blower et al. (2002), the probability of a plane intersecting a given sphere is proportional to the sphere's radius, R. Cross-sections of radius r may be obtained from any sphere with a radius greater than or equal to r. We may now write a general expression for the probability of obtaining a cross-section of radius r from the whole distribution [which is denoted $F(R)$]:

$$f(r) = \int_r^\infty F(R) R \frac{1}{R} \frac{r}{\sqrt{R^2 - r^2}} dR\,, \tag{11}$$

which is formula (A7) in Blower et al. (2002). That is to say, $f(r)$ is the probability of finding a bubble of radius R, multiplied by the probability of intersecting this bubble, multiplied by the probability of obtaining a slice of radius r from this bubble, integrated over the range of $R \geq r$. A first example is given by the so-called monodisperse bubble size distribution (BSD) which are bubbles of constant radius R and therefore

$$F(R) = \frac{1}{R}\,, \tag{12}$$

which is defined in the interval $[0, R]$ and

$$f(r) = \frac{r}{\sqrt{R^2 - r^2} R}\,, \tag{13}$$

which is defined in the interval $[0, R]$, see equation (A4) in Blower et al. (2002). The average value of the radius of the 2D-slices is

$$\overline{r} = 1/4\, R\pi\,, \tag{14}$$

the variance is

$$\sigma^2 = 2/3\, R^2 - 1/16\, R^2 \pi^2\,, \tag{15}$$

and finally,

$$\text{Skewness} = -1.151, \quad \text{Kurtosis} = 0.493\,. \tag{16}$$

3.1. *PVT stereology*

In order to find our $F(R)$, we now analyze the distribution in effective radius R of the 3D PVT. We assume that the volume of each cell, v, is

$$v = \frac{4}{3}\pi R^3\,. \tag{17}$$

In the following, we derive the PDF for the radius and related quantities relative to the Ferenc-Néda function. The PDF as a function of the radius according to the rule of change of variables (equation 10), is obtained from equation (4) on inserting $d = 3$:

$$F(R) = \frac{400000}{243}\,\pi^5 R^{14} \mathrm{e}^{-\frac{20}{3}\,\pi\,R^3}\,. \tag{18}$$

The average radius is

$$\overline{R} = 0.6065\,, \tag{19}$$

and the variance is

$$\sigma^2(R) = 0.00853\,. \tag{20}$$

TABLE 2

THE PARAMETERS OF $f(r)$, EQUATION (22), RELATIVE TO THE PVT CASE

Parameter	Value
Mean	0.4874
Variance	0.02475
Mode	0.553
Skewness	−0.5229
Kurtosis	−0.1115

TABLE 3

PARAMETERS OF $f(x, b)$, EQUATION (27), RELATIVE TO THE PVT CASE

Parameter	$b = 2.051$	$b = 34$
Mean	1.	16.57 Mpc
Variance	0.104	28.62 Mpc^2
Mode	1.134	18.80 Mpc

The introduction of the scale factor, b, with the new variable $R = R'/b$ transforms equation (18) into

$$F(R', b) = \frac{400000\,\pi^5 R'^{14} \mathrm{e}^{-\frac{20}{3}\,\frac{\pi R'^3}{b^3}}}{243\,b^{15}}\,. \tag{21}$$

We now have $F(R)$ as given by equation (18) and the fundamental integral (equation 11), as derived in Ferraro & Zaninetti (2011), is

$$f(r) = 2/3\,K\,\sqrt[6]{3}\sqrt[3]{10}\sqrt[3]{\pi} r G^{4,1}_{3,5}\left(\frac{100}{9}\,\pi^2 r^6 \,\middle|\, \begin{matrix} 5/6,1/6,1/2 \\ 7/3,2/3,1/3,0,\frac{17}{6} \end{matrix}\right) \quad \text{with} \quad 0 \le r \le 1\,, \tag{22}$$

where K is a constant,

$$K = 1.6485\,, \tag{23}$$

and the Meijer G-function is defined as in Meijer (1936, 1941); Olver et al. (2010). Details on the real or complex parameters of the Meijer G-function are given in the Appendix. Table 2 shows the average value, variance, mode, skewness, and kurtosis of the already derived $f(r)$.

Asymptotic series are

$$f(r) \sim 2.7855\,r \quad \text{when} \quad r \to 0\,, \tag{24}$$

and

$$f(r) \sim -0.006\,(r-1) + 0.136\,(r-1)^2 \quad \text{when} \quad r \to 1\,. \tag{25}$$

The distribution function (DF) is

$$DF(r) = \frac{1}{90}\,K\,3^{5/6}10^{2/3} G^{4,2}_{4,6}\left(\frac{100}{9}\,\pi^2 r^6 \,\middle|\, \begin{matrix} 1,7/6,1/2,5/6 \\ 8/3,1,2/3,1/3,\frac{19}{6},0 \end{matrix}\right) \frac{1}{\sqrt[3]{\pi}} \quad \text{when} \quad 0 \le r \le 1. \tag{26}$$

The PDF is defined in the interval $0 \le r \le 1$. In order to make a comparison with a normalized sample which has a unit mean or an astronomical sample which has the mean expressed in Mpc, a transformation of scale should be introduced. The change of variable is $r = x/b$ and the resulting PDF is

$$f(x, b) = \frac{2}{3}\,K\,\sqrt[6]{3}\sqrt[3]{10}\sqrt[3]{\pi} x G^{4,1}_{3,5}\left(\frac{100}{9}\,\frac{\pi^2 x^6}{b^6} \,\middle|\, \begin{matrix} 5/6,1/6,1/2 \\ 7/3,2/3,1/3,0,\frac{17}{6} \end{matrix}\right) (\frac{1}{b})^2 \quad \text{when} \quad 0 \le r \le b. \tag{27}$$

As an example, Table 3 shows the statistical parameters for two different values of b. The skewness and kurtosis do not change with a transformation of scale.

We briefly recall that a PDF $f(x)$ is the first derivative of a distribution function (DF) $F(x)$ with respect to x. When the DF is unknown but the PDF known, we have

$$F(x) = \int_0^x f(x)dx\,. \tag{28}$$

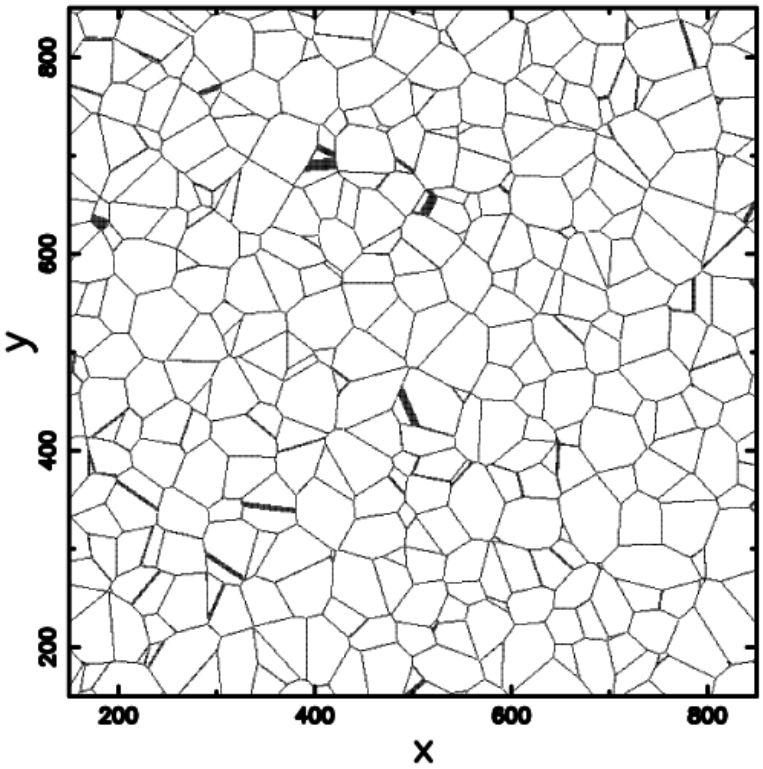

Fig. 1. PVT diagram $V_p(2,3)$ when 789 2D cells generated by 15000 3D seeds are considered.

The survival function (SF) $S(x)$ is

$$S(x) = 1 - F(x)\,, \tag{29}$$

and represents the probability that the variate takes a value greater than x. The SF with the scaling parameter b is

$$SF(x,b) = 1 - 0.01831\, 3^{5/6} 10^{2/3} G^{4,2}_{4,6}\left(\frac{100}{9}\,\frac{x^6\pi^2}{b^6}\,\Big|\,{}^{1,7/6,1/2,5/6}_{8/3,1,2/3,1/3,\frac{19}{6},0}\right)\frac{1}{\sqrt[3]{\pi}}\,, \quad \text{with} \quad 0 \le r \le b\,. \tag{30}$$

A first application can be a comparison between the real distribution of radii of $V_p(2,3)$, see Figure 1, and the already obtained rescaled PDF $f(x,b)$. The fit with the rescaled $f(x,b)$ is shown in Figure 2 and Table 4 shows the χ^2 of three different fitting functions.

The PDF f_A of the areas of $V_p(2,3)$ can be obtained from $f(r)$ by means of the transformation (Ferraro & Zaninetti 2011),

$$f_A(A) = f(r)\left(\frac{A}{\pi}\right)^{1/2}\frac{\pi^{-1/2}}{2}A^{-1/2}\,, \tag{31}$$

that is,

$$f_A(A) = 0.549\,\sqrt[6]{3}\sqrt[3]{10}G^{\,4,1}_{3,5}\left(\frac{100}{9}\,\frac{A^3}{\pi}\,\Big|\,{}^{5/6,1/6,1/2}_{7/3,2/3,1/3,0,\frac{17}{6}}\right)\pi^{-2/3}\,. \tag{32}$$

The already derived $f_A(A)$ has average value, variance, mode, skewness and kurtosis as shown in Table 5.

Since, for r close to 0, $f(r) \sim r$ from equation (32) it follows that $f_A(0) \neq 0$, in particular $f_A(0) = 0.443$ and Figure 3 shows the graph of f_A.

The previous figure shows that sections through 3-dimensional Voronoi tessellations are not themselves 2-dimensional Voronoi tessellations because $f_A(0)$ has a finite value rather than 0, as does the 2D area distribution; this fact can be considered a numerical demonstration in agreement with Chiu et al. (1996). The distribution

TABLE 4

THE VALUES OF χ^2 FOR THE CELL NORMALIZED AREA-DISTRIBUTION OF $V_p(2,3)$[a]

PDF	Parameters	χ^2
$H(x;c)$ (equation 1)	$c = 5.8$	250.8
$f(x;d)$ (equation 4)	$d = 3.53$	250.8
$f(x;b)$ (equation 27)	$b = 2.0514$	127

[a]The number of 2D cells is 789, the 3D seeds are 15000 and the number of bins in the histogram is 30.

TABLE 5

PARAMETERS OF $f_A(A)$, EQUATION (32), RELATIVE TO THE PVT CASE

Parameter	Value
Mean	0.824
Variance	0.204
Mode	0.858
Skewness	0.278
Kurtosis	−0.337

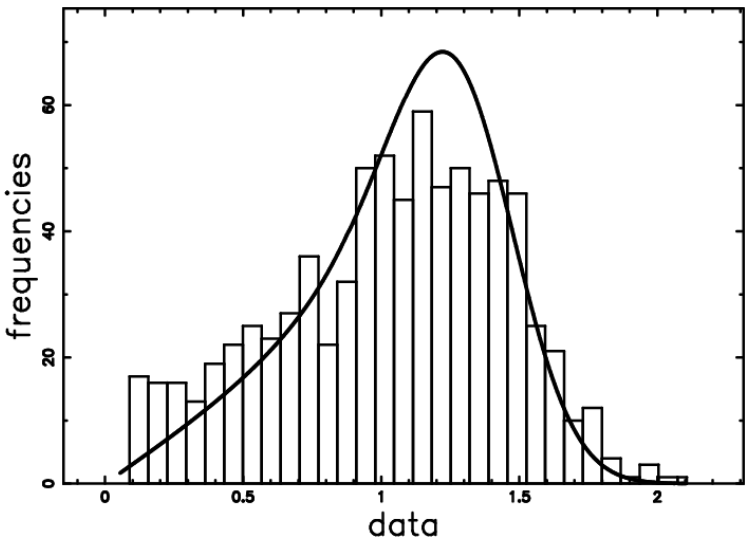

Fig. 2. Histogram (step-diagram) of PVT $V_p(2,3)$ when 789 2D cells, generated by 15000 3D seeds, are considered. The superposition of the $f(x,b)$, equation (27), is displayed.

function F_A is given by

$$F_A = 0.018\, 3^{5/6} 10^{2/3} G^{4,2}_{4,6}\left(\frac{100}{9}\,\frac{A^3}{\pi}\,\Big|\,{}^{1,7/6,1/2,5/6}_{8/3,1,2/3,1/3,\frac{19}{6},0}\right)\frac{1}{\sqrt[3]{\pi}}\,. \tag{33}$$

Consider a three-dimensional Poisson-Voronoi diagram and suppose it intersects a randomly oriented plane γ: the resulting cross sections are polygons.

A comparison between F_A and the area of the irregular polygons is shown in Figure 4. In this case the number of seeds is 300000 and we processed 100168 irregular polygons obtained by adding together results of cuts by 41 triples of mutually perpendicular planes. The maximum distance between the two curves is $d_{\max} = 0.039$.

As concerns the linear dimension, in our approximation the two-dimensional cells were considered circles and thus, for consistency, the radius r of an irregular polygon was defined as

$$r = \left(\frac{A}{\pi}\right)^{1/2}\,, \tag{34}$$

that is, r is the radius of a circle with the same area, A, as the polygon. The assumption of sphericity can be

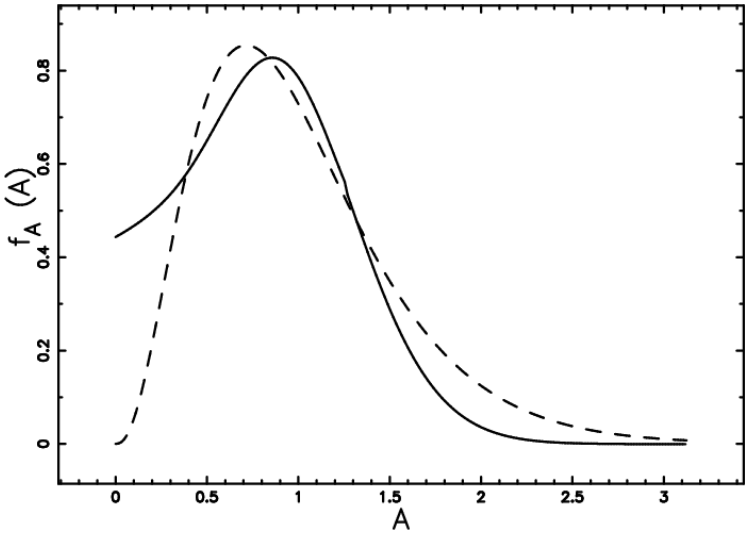

Fig. 3. The PDF f_A, equation (32), as a function of A (full line) and $FN(x;d)$, equation (4), when $d = 2$ (dotted line).

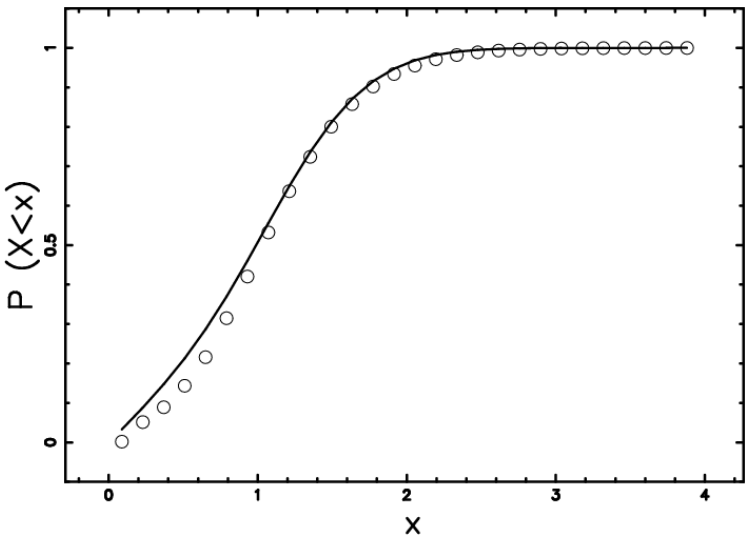

Fig. 4. Comparison between data (empty circles) and theoretical curve (continuous line) of the distribution of areas of the planar cross sections.

considered an axiom of the theory here presented, but for a more realistic situation the stereological results will be far more complex.

4. STATISTICS OF THE VOIDS

This section first processes 1024 observed cosmic voids and then derives the same results from the stereological point of view.

4.1. *Observed statistics*

The distribution of the effective radius and the radius of the maximum enclosed sphere between galaxies of the Sloan Digital Sky Survey Data Release 7 (SDSS DR7) has been reported in Pan et al. (2011). This catalog contains 1054 voids: Table 6 shows the basic statistical parameters of the effective radius, and Table 7, the radius of the maximum enclosed sphere.

TABLE 6

THE STATISTICAL PARAMETERS OF THE EFFECTIVE RADIUS IN SDSS DR7

Parameter	Value
Elements	1024
Mean	18.23 h^{-1} Mpc
Variance	23.32 h^{-2} Mpc^2
Standard deviation	4.82 h^{-1} Mpc
Skewness	0.51
Kurtosis	0.038
Maximum value	34.12 h^{-1} Mpc
Minimum value	9.9 h^{-1} Mpc

TABLE 7

THE STATISTICAL PARAMETERS OF THE RADIUS OF THE MAXIMAL ENCLOSED SPHERE IN SDSS DR7

Parameter	Value
Elements	1054
Mean	12.95 h^{-1} Mpc
Variance	6.99 h^{-2} Mpc^2
Standard deviation	2.64 h^{-1} Mpc
Skewness	1.47
Kurtosis	2.401
Maximum value	25.69 h^{-1} Mpc
Minimum value	10 h^{-1} Mpc

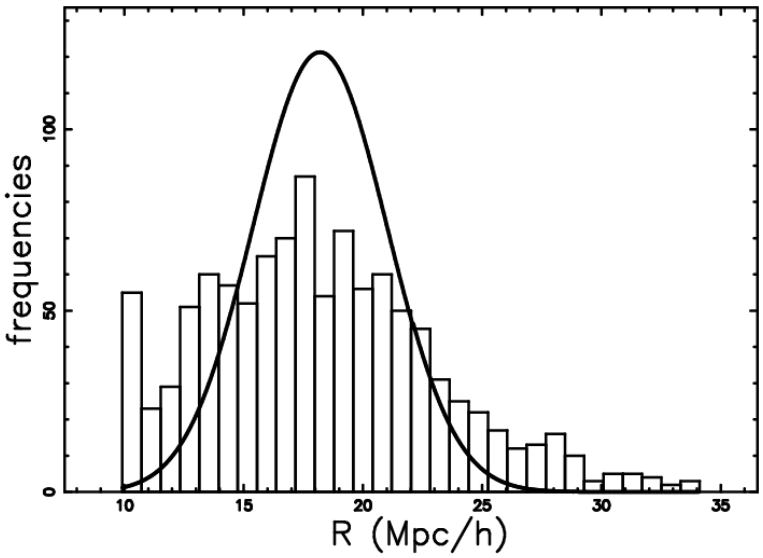

Fig. 5. Histogram (step-diagram) of the effective radius in SDSS DR7 with a superposition of the PDF of radius of the PVT spheres, $F(R, b)$, as represented by equation (21). The number of bins is 30, and b=30.05 Mpc.

4.2. *PVT statistics*

Figure 5 shows a superposition of the effective radius of the voids in the SDSS DR7 with the curve of the theoretical PDF of the radii, $F(R, b)$, as given by equation (21). Table 8 shows the theoretical statistical parameters.

Table 9 shows the values of χ^2 for the main PDFs here considered. The statistics of the voids can also be visualized through the SF, see an application to the 2dFGRS as given by Patiri et al. (2006); von Benda-Beckmann & Müller (2008).

The statistics of the voids between galaxies have been also analyzed in von Benda-Beckmann & Müller (2008) with the following self-similar SF denoted by $S_{\rm SS}$,

$$S_{\rm SS} = \mathrm{e}^{-\left(\frac{R}{s_1\lambda}\right)^{p_1}-\left(\frac{R}{s_2\lambda}\right)^{p_2}}, \tag{35}$$

TABLE 8

THE STATISTICAL PARAMETERS OF THE THEORETICAL RADIUS OF THE PVT SPHERES AS REPRESENTED BY EQUATION (21) WHEN b=30.05 Mpc

Parameter	Value
Mean	18.23 h^{-1} Mpc
Variance	7.70 h^{-2} Mpc^2
Standard deviation	2.77 h^{-1} Mpc
Mode	18.49 h^{-1} Mpc
Skewness	0.0142
Kurtosis	−0.0514

TABLE 9

VALUES OF χ^2 FOR THE EFFECTIVE RADIUS IN SDSS DR7[a]

PDF	Parameters	χ^2
$H(x;c)$, (eq. 1)	$c = 14.24$	53
$f(x;d)$, (eq. 4)	$d = 9.1$	53
$f(x,b)$, (eq. 27)	$b = 2.051$	182
$F(R,b)$, (eq. 21)	$b = 1.648$	407
$F_K(R,b,c)$, (eq. 36)	$b = 31.33$ $c = 1.76$	66.121

[a]Values for different distributions when the number of bins is 30. In this comparison, the averaged value of the astronomical radii is one.

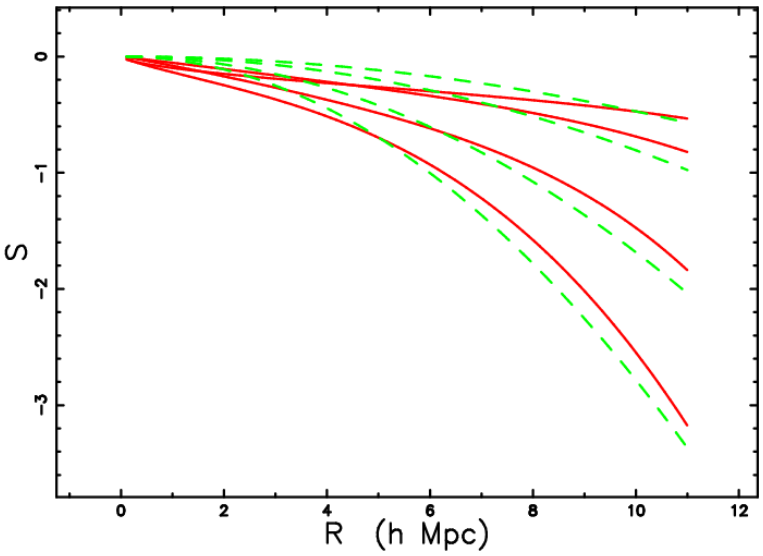

Fig. 6. The survival function, S_{SS}, for the self-similar distribution of radius of $N/S1$, $N/S2$, $N/S3$ and $N/S4$, as reported in Figure 4 of von Benda-Beckmann & Müller (2008) (full red lines), as represented by equation (35). The survival function, $SF(x,b)$, of the radius of the distribution which involves the Meijer G-function for $V_p(2,3)$ as represented by equation (30) when $b = 12$ Mpc, $b = 14$ Mpc, $b = 17$ Mpc, and $b = 19$ Mpc (dashed green lines). The color figure can be viewed online.

where λ is the mean separation between galaxies, s_1 and s_2 are two length factors, and p_1 and p_2 two powers. A final comparison between the four samples of void size statistics as represented in Figure 4 of von Benda-Beckmann & Müller (2008) and our survival function of the radius for $V_p(2,3)$ as given by equation (30) is shown in Figure 6.

More details as well the PDF of the self-similar distribution can be found in Zaninetti (2010).

5. NPVT STATISTICS

An example of non-NPVT is represented by a distribution in volume which follows a Kiang function as given by equation (1). The case of PVT volumes indicates $c = 5$, see equation (8), or $c = 6$, the so called Kiang conjecture; we will take c as a variable. The resulting distribution in radius once the scaling parameter b is

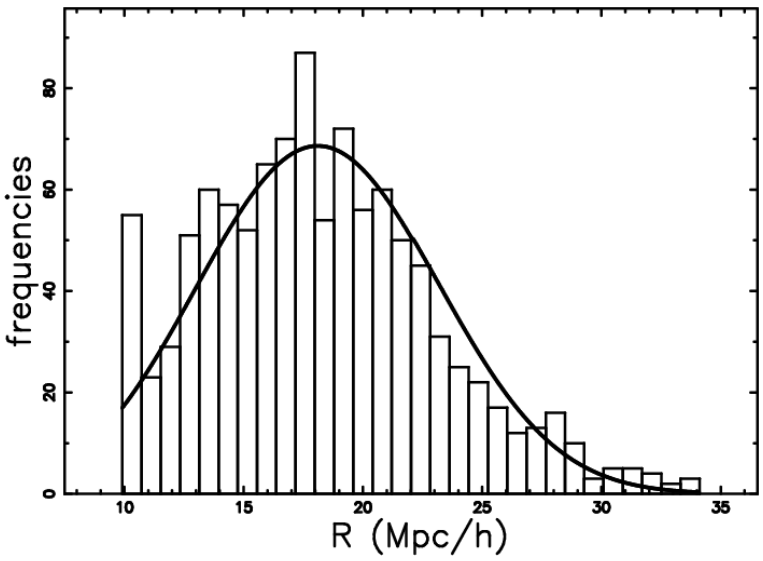

Fig. 7. Histogram (step-diagram) of the effective radius in the SDSS DR7 with a superposition of the PDF of radius of the NPVT spheres, $F_K(R,b,c)$, as represented by equation (36). The number of bins is 30, $b = 31.33$ Mpc, and $c = 1.768$.

introduced is

$$F_K(R,b,c) = \frac{4\,c\left(4/3\;\frac{c\pi\,R^3}{b^3}\right)^{c-1}\mathrm{e}^{-4/3\;\frac{c\pi\,R^3}{b^3}}\pi\,R^2}{\Gamma\,(c)\,b^3}\,. \tag{36}$$

The average radius is

$$\overline{R} = \frac{\sqrt[3]{2}\sqrt[3]{3}b\Gamma\,(1/3+c)}{2\,\sqrt[3]{c}\sqrt[3]{\pi}\Gamma\,(c)}\,, \tag{37}$$

and the variance is

$$\sigma^2(R) = \frac{-3^{2/3}2^{2/3}b^2\left(-\Gamma\,(2/3+c)\,\Gamma\,(c)+(\Gamma\,(1/3+c))^2\right)}{4\,c^{2/3}\pi^{2/3}\,(\Gamma\,(c))^2}\,. \tag{38}$$

The skewness is

$$\gamma = \frac{(\Gamma\,(c))^3\,c - 3\,\Gamma\,(c)\,\Gamma\,(1/3+c)\,\Gamma\,(2/3+c) + 2\,(\Gamma\,(1/3+c))^3}{\left(\Gamma\,(2/3+c)\,\Gamma\,(c)-(\Gamma\,(1/3+c))^2\right)^{3/2}}\,, \tag{39}$$

and the kurtosis is given by a complicated analytic expression. Figure 7 shows a superposition of the effective radii of the voids in SDSS DR7 with the curve of the theoretical PDF in the radius, $F_K(R,b,c)$, as represented by equation (36). Table 9 shows the values of χ^2. Table 10 shows the theoretical statistical parameters.

The result of the integration of the fundamental equation (11) inserting $c = 2$ gives the following PDF for the radius of the cuts

$$f(r)_{\mathrm{NPVTK}} = 3.4148\,\sqrt[6]{3}\sqrt[3]{\pi}r2^{2/3}G^{4,0}_{2,4}\left(\frac{16}{9}\,\pi^2r^6\,\Big|\,{}^{1/6,1/2}_{4/3,2/3,1/3,0}\right)\,,\quad \text{when}\quad 0\le r\le 1\,. \tag{40}$$

The statistics of NPVT cuts with $c = 2$ are shown in Table 11.

On introducing the scaling parameter b, the PDF which describes the radius of the cut becomes

$$f(x,b)_{\mathrm{NPVTK}} = 3.4148\,\sqrt[6]{3}\sqrt[3]{\pi}x2^{2/3}G^{4,0}_{2,4}\left(\frac{16}{9}\,\frac{\pi^2x^6}{b^6}\,\Big|\,{}^{1/6,1/2}_{4/3,2/3,1/3,0}\right)b^{-2}\,,\quad \text{with}\quad 0\le r\le b\,. \tag{41}$$

TABLE 10

THE STATISTICAL PARAMETERS OF THE THEORETICALRADIUS OF THE NPVT SPHERES AS REPRESENTED BY EQUATION (36) WHEN $b = 31.33$ Mpc AND $c = 1.768$

Parameter	Value
Mean	18.23 h^{-1} Mpc
Variance	23.31 h^{-2} Mpc^2
Standard deviation	4.82 h^{-1} Mpc
Skewness	0.072
Kurtosis	−0.162

TABLE 11

NPVT PARAMETERS OF $f(r)_{\rm NPVTK}$, EQUATION (40)

Parameter	Value
Mean	0.488
Variance	0.0323
Mode	0.517
Skewness	−0.114
Kurtosis	2.614

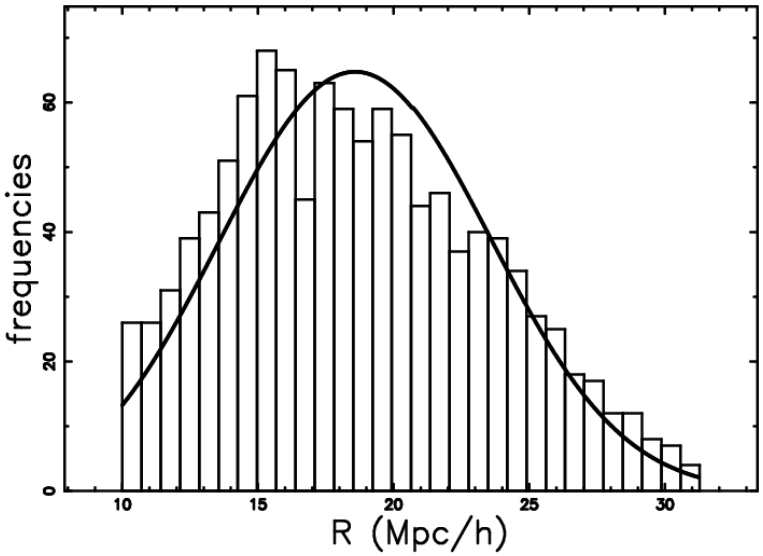

Fig. 8. Histogram (step-diagram) of the simulated effective radius of SDSS DR7 with a superposition of the PDF of radius of the PVT spheres as represented by equation (36). The artificial sample has a minimum value of 10/h Mpc, the number of bins is 30, $b = 31.5$/h Mpc, and $c = 1.3$.

The SF of the *second* NPVT case, $SF_{\rm NPVTK}$, with the scaling parameter b, is

$$SF(x,b)_{\rm NPVTK} = 1 - 0.2845\, 3^{5/6}\, \sqrt[3]{2} G^{4,1}_{3,5}\left(\frac{16}{9}\,\frac{\pi^2 x^6}{b^6}\,\Big|^{1,1/2,5/6}_{5/3,1,2/3,1/3,0}\right)\frac{1}{\sqrt[3]{\pi}}\,, \quad \text{with} \quad 0 \le r \le b\,. \tag{42}$$

A careful exploration of the distribution in effective radius of SDSS DR7 reveals that the detected voids have radius ≥10/h Mpc. This observational fact demands the generation of random numbers in the distribution of radii of the 3D cells as given by equation (36) with a minimum value of 10/h Mpc. The artificial sample is generated through a numerical computation of the inverse function (Brandt 1998) and displayed in Figure 8; the sample statistics are shown in Table 12.

TABLE 12

STATISTICAL PARAMETERS OF THE ARTIFICIALLY GENERATED RADIUS WITH A LOWER BOUND OF 10/h Mpc, $c = 1.3$ AND $b = 31.5$/h Mpc

Parameter	Value
Mean	18.69 h^{-1} Mpc
Variance	22.74 h^{-2} Mpc^2
Standard deviation	4.76 h^{-1} Mpc
Skewness	0.33
Kurtosis	−0.623
Maximum value	31.27 h^{-1} Mpc
Minimum value	10 h^{-1} Mpc

6. CONCLUSIONS

PVT Statistics. The approach as given by the stereology to the PDF of the radii of the circles which result from the intersection between a plane and a randomly disposed spheres of radius R is actually limited to the case of mono-disperse spheres of radius R and to a power law with radius $\propto R^{-\alpha}$ (Blower et al. 2002). Here adopting the same type of demonstration we simply substitute into equation 11 a new distribution for the generalized radii, (R), of PVT. The resulting distribution of the radii, (r), of the circles of intersection involves the Meijer G-function. A first test on this new PDF for the radii was performed on the 2dFGRS catalog and the theoretical $V_p(2, 3)$ cells were compared with other fitting functions, see Figure 6.

NPVT Statistics. Among the infinite number of 3D seeds which are non-Poissonian, we selected a distribution in volume which follows a Kiang function as given by equation (1) with $c \approx 2$.

A careful comparison with the measured effective radii permits us to say that the NPVT case here considered is a good model because it can reproduce the 3D average radius and the variance, see Table 10. The model for the effective radius of the voids as given by the Kiang distribution of volumes with c variable can also be used to generate an artificial sample of the effective radius of the voids, see Figure 8 and Table 12.

I would like to thank the anonymous referee for constructive comments on the text and Mario Ferraro for positive discussions on the Voronoi Diagrams.

APPENDIX. THE MEIJER G-FUNCTION

In general the Meijer G-function is defined by the following Mellin-Barnes type integral on the complex plane,

$$ccG_{p,q}^{m,n}(z) \equiv G_{p,q}^{m,n}\left(z \left| \begin{array}{c} c(a_i)_1^p \\ \\ (b_j)_1^q \end{array} \right.\right) \equiv G_{p,q}^{m,n}\left(z \left| \begin{array}{c} a_1, \ldots, a_p \\ \\ b_1, \ldots, b_q \end{array} \right.\right) = \frac{1}{2\pi i} \int_{\mathcal{L}} \frac{\prod_{j=1}^{m} \Gamma(b_j + s) \prod_{j=1}^{n} \Gamma(1 - a_j - s)}{\prod_{j=n+1}^{p} \Gamma(a_j + s) \prod_{j=m+1}^{q} \Gamma(1 - b_j - s)} z^{-s} ds \,, \tag{43}$$

where the contour of integration $\mathcal{L}$ is arranged to lie between the poles of $\Gamma(a_i + s)$ and the poles of $\Gamma(b_j + s)$. The G-function is defined under the following hypothesis.

- $0 \leq m \leq q,\ 0 \leq n \leq p,$ and $p \leq q - 1$;
- $z \neq 0$;
- no pair of b_j, j distinct, $j =, 2, \ldots, m$ differ by an integer or zero;

- the parameters $a_i \in \mathrm{C}$ and $b_j \in \mathrm{C}$ are such that no pole of $\Gamma(b_j + s),\ j = 1, 2, \ldots, m$ coincides with any pole of $\Gamma(a_i + s),\ i = 1, 2, \ldots, n$;
- $a_i - b_j \neq 1, 2, 3, \ldots$ for $i = 1, 2, \ldots, n$ and $j = 1, 2, \ldots, m$; and
- if $p = q$, then the definition makes sense only for $|z| < 1$ (Meijer 1936, 1941; Ho, James, & Lau 2007; Olver et al. 2010).

REFERENCES

Abazajian, K. N., et al. 2009, ApJS, 182, 543
Barrow, J. D., & Coles, P. 1990, MNRAS, 244, 188
Bernardeau, F., & van de Weygaert, R. 1996, MNRAS, 279, 693
Blower, J., Keating, J., Mader, H., & Phillips, J. 2002, J. Volcanol. Geotherm. Res., 120, 1
Brandt, S. 1998, Data Analysis: Statistical and Computational Methods for Scientists and Engineers (New York: Springer-Verlag)
Chiu, S. N., Weygaert, R. V. D., & Stoyan, D. 1996, Adv. in Appl. Prob., 28, 356
Coles, P. 1991, Nature, 349, 288
Colless, M., et al. 2001, MNRAS, 328, 1039
Ebeling, H., & Wiedenmann, G. 1993, Phys. Rep., 47, 704
Elyiv, A., Melnyk, O., & Vavilova, I. 2009, MNRAS, 394, 1409
Ferenc, J.-S., & Néda, Z. 2007, Physica A: Statistical Mechanics and its Applications, 385, 518
Ferraro, M., & Zaninetti, L. 2011, Phys. Rev. E., 84, 041107
Geller, M. J., & Huchra, J. P. 1989, Science, 246, 897
Goldwirth, D. S., da Costa, L. N., & van de Weygaert, R. 1995, MNRAS, 275, 1185
Ho, M.-W., James, L. F., & Lau, J. W. 2007, arXiv:0708.0619
Icke, V., & van de Weygaert, R. 1987, A&A, 184, 16
Ikeuchi, S., & Turner, E. L. 1991, MNRAS, 250, 519
Kiang, T. 1966, Zert. Astrophys., 64, 433
Marinoni, C., Davis, M., Newman, J. A., & Coil, A. L. 2002, ApJ, 580, 122
Meijer, C. 1936, Nieuw Arch. Wiskd., 18, 10
_____. 1941, Proc. Akad. Wet. Amsterdam, 44, 1062
Melnyk, O. V., Elyiv, A. A., & Vavilova, I. B. 2006, Kinematika i Fizika Nebesnykh Tel, 22, 283
Møller, J. 1989, Adv. Appl. Prob., 21, 37
_____. 1994, Lectures on Random Voronoi Tessellations (Lecture Notes in Statistics, 87; New York: Springer-Verlag)
Okabe, A., Boots, B., & Sugihara, K. 1992, Spatial Tessellations. Concepts and Applications of Voronoi Diagrams (New York: Wiley)
Olver, F., Lozier, D., Boisvert, R., & Clark, C. 2010, NIST Handbook of Mathematical Functions (Cambridge: Cambridge Univ. Press)
Pan, D. C., Vogeley, M. S., Hoyle, F., Choi, Y.-Y., & Park, C. 2011, arXiv:1103.4156
Patiri, S. G., Betancort-Rijo, J. E., Prada, F., Klypin, A., & Gottlöber, S. 2006, MNRAS, 369, 335
Pierre, M. 1990, A&A, 229, 7
Schaap, W. E., & van de Weygaert, R. 2000, A&A, 363, L29
Subba-Rao, M. U., & Szalay, A. S. 1992, ApJ, 391, 483
van de Weygaert, R. 1991a, MNRAS, 249, 159
_____. 1991b, PhD. Thesis, University of Leiden, The Netherlands
_____. 1994, A&A, 283, 361
_____. 2002, arXiv:astro-ph/0206427
_____. 2003, in Statistical Challenges in Astronomy, ed. E. D. Feigelson, & G. Jogesh Babu (Berlin: Springer-Verlag), 156
van de Weygaert, R., & Icke, V. 1989, A&A, 213, 1
van de Weygaert, R., & Schaap, W. 2009, Lect. Notes Phys., 665, 291
von Benda-Beckmann, A. M., & Müller, V. 2008, MNRAS, 384, 1189
Voronoi, G. 1907, J. Reine Angew. Math., 133, 97
_____. 1908, J. Reine Angew. Math., 134, 198
York, D. G., et al. 2000, AJ, 120, 1579
Zaninetti, L. 1991, A&A, 246, 291
_____. 2006, Chinese J. Astron. Astrophys., 6, 387
_____. 2010, Serbian Astr. Jour., 181, 19

L. Zaninetti: Dipartimento di Fisica, Universitá degli Studi di Torino, Via Pietro Giuria 1, 10125 Torino, Italy (zaninetti@ph.unito.it).